YALE
PEABODY
MUSEUM

JOURNAL OF MARINE RESEARCH

The *Journal of Marine Research,* one of the oldest journals in American marine science, published important peer-reviewed original research on a broad array of topics in physical, biological, and chemical oceanography vital to the academic oceanographic community in the long and rich tradition of the Sears Foundation for Marine Research at Yale University.

An archive of all issues from 1937 to 2021 (Volume 1–79) are available through EliScholar, a digital platform for scholarly publishing provided by Yale University Library at https://elischolar.library.yale.edu/.

Requests for permission to clear rights for use of this content should be directed to the authors, their estates, or other representatives. The *Journal of Marine Research* has no contact information beyond the affiliations listed in the published articles. We ask that you provide attribution to the *Journal of Marine Research.*

Yale University provides access to these materials for educational and research purposes only. Copyright or other proprietary rights to content contained in this document may be held by individuals or entities other than, or in addition to, Yale University. You are solely responsible for determining the ownership of the copyright, and for obtaining permission for your intended use. Yale University makes no warranty that your distribution, reproduction, or other use of these materials will not infringe the rights of third parties.

Large-scale SST anomalies associated with subtropical fronts in the western North Atlantic during FASINEX

by George R. Halliwell, Jr.[1] and Peter Cornillon[1]

ABSTRACT

We describe the large-scale variability of sea surface temperature (T_s) and fronts in the western North Atlantic Subtropical Convergence Zone from January–June 1986 within an approximately 11° longitude by 10° latitude domain. Fronts were primarily found within interconnected bands separated by <500 km that tended to be located on the periphery of anisotropic T_s spatial anomaly features that propagated westward at about 3 km day^{-1}. Relatively weak and strong (small or large $|\nabla T_s|$) segments of the dominant zonally-oriented frontal band (the Subtropical Frontal Zone, or SFZ) shifted westward with these anomaly features, which had characteristic peak-to-peak space scales of up to ≈800 km in the minor axis direction (NW-SE) and time scales of up to ≈275 days, both larger than the scales of mesoscale eddies observed during earlier experiments. Both the main and seasonal thermoclines tended to be elevated (depressed) by several tens of meters beneath cold (warm) anomaly features, suggesting that the influence of eddies on T_s and fronts extends to larger space and longer time scales than those resolved in earlier studies. Because of the very limited spatial and temporal coverage of available subsurface data, however, this relationship could not be verified conclusively. Properties of the anomaly features were consistent with the dispersion of lowest-mode internal Rossby waves, and they were apparently not generated or significantly influenced by wind-driven Ekman transport. A much longer data set, including altimetry and subsurface data, will be required to verify that eddies influence T_s and fronts at these large scales, and if so, to determine the physical processes behind this influence.

1. Introduction

The large-scale variability of sea surface temperature (T_s) and of the Subtropical Frontal Zone (SFZ) in the western North Atlantic Ocean between January and June 1986 was studied by Halliwell and Cornillon (1990a,b, henceforth referred to as HC1 and HC2) as part of the Frontal Air-Sea Interaction Experiment (FASINEX) (Stage and Weller, 1985, 1986). The SFZ is a predominantly zonal band of relatively large $|\nabla T_s|$ a few degrees of latitude wide (HC1) that appears in sufficiently long temporal averages of the T_s field (Roden, 1980; Van Woert, 1983, HC1). The SFZ is located within the Subtropical Convergence Zone (STCZ), a zonally-oriented band typically centered between 25N and 30N in the FASINEX region where meridional conver-

gence of surface wind-driven Ekman transport exists between the Westerlies to the north and the Trade Winds to the south. One or more oceanic surface temperature fronts are usually observed within the SFZ, distinguished by jumps of up to 3°C within a distance of several kilometers (Voorhis, 1969; Van Woert, 1982; Niiler and Reynolds, 1984). The distinction between fronts and frontal zones is discussed in general by Fedorov (1983), and it is discussed for subtropical convergence zones by Roden (1980), Niiler and Reynolds (1984), and Halliwell (1989).

Deformation in the horizontal current field caused by mesoscale eddies with peak-to-peak space scales of ≈100–400 km and time scales of ≈100 days often produces frontogenesis and frontolysis, and often deforms existing fronts (Van Woert, 1982; Voorhis *et al.*, 1976). (All space and time scales will be peak-to-peak scales unless otherwise noted.) Currents caused by smaller, shorter-period submesoscale eddies also affect the fronts (Leetmaa and Voorhis, 1978; Voorhis and Bruce, 1982). In this paper, we describe the distribution and variability of surface temperature fronts (including the dominant SFZ), and the T_s variability associated with these fronts, during FASINEX within the same 11° longitude by 10° latitude domain used in HC1 and HC2. Data limitations prohibited us from accurately resolving variability with space scales smaller than about 300–400 km, the size of the largest mesoscale eddies. Since the T_s variability described in this paper is dominated by variability substantially larger than the mesoscale eddies, we will use the term "large-scale" to identify it. We will refer to space scales much larger than the size of the analysis domain (≫1100 km), which we could not resolve, as secular scales.

We show that fronts tend to be found on the periphery of westward-propagating spatial T_s anomaly features with scales of up to ≈800 km and ≈275 days. The evidence presented here indicates that the influence of underlying eddies on T_s and the fronts may extend to the larger space and time scales resolved in this study. Unfortunately, the time interval of this study was too short, and insufficient supporting data (subsurface, satellite altimetry, . . .) were available, either to conclusively prove the existence of a large-scale eddy influence, or to identify the physical processes responsible for this influence if it does exist. Whatever processes are involved, these westward-propagating anomaly features dominated the T_s variability at large scales during FASINEX, making it difficult to detect the expected response of fronts in the STCZ to the meridional convergence of Ekman transport.

2. The data set

In previous studies, we have described basic statistical properties of the wind and satellite-derived T_s fields during FASINEX (HC1), and quantitatively analyzed the contributions of some physical mechanisms to both the large-scale upper-ocean heat balance and the observed large-scale variability of the SFZ (HC2). These studies focused on an approximately 11° longitude by 10° latitude domain in the western

North Atlantic containing the FASINEX site. We use this same data set for our present analyses, which includes 5-day maps of T_s on a 46 × 40 grid with a resolution of 0.25° in both latitude and longitude derived from NOAA-7 and NOAA-9 AVHRR/2 infrared images, and 5-day averaged Fleet Numerical Oceanography Center (FNOC) wind stress and wind stress curl maps on a 5 × 5 grid with a 2.5° resolution in both latitude and longitude. We refer the reader to HC1 for a complete description of this data set. We also use FASINEX ship-of-opportunity XBT data (Evans *et al.*, 1986) and FASINEX current meter data (Pennington *et al.*, 1988) to search for possible relationships between the observed large-scale anomaly features and internal oceanic eddies.

The T_s maps were spatially smoothed with a 9 × 9 point two-dimensional Hanning window (HC2), which reduces the variance of T_s by <20% for λ ≥ 500 km, by about 50% for λ ≈ 300 km, and by >90% for λ ≤ 100 km. Smoothing was necessary because smaller-scale variability in the maps was often poorly resolved due to cloud cover. Since large-scale features in these smoothed maps were dominated by periods ≫10 days, we analyzed eight 25-day maps, each the average of five 5-day maps and separated by 20 days. The averaging and separation intervals were selected to resolve the large-scale variability during FASINEX as well as possible with a small number of T_s maps.

3. Fronts

a. Distribution. Böhm (1988) digitized frontal paths using individual AVHRR images, then plotted monthly compilations of these paths between October 1982 and June 1986. We present a compilation of these fronts, along with a contour plot of $|\nabla T_s|$, for the second of our eight 25-day intervals (31 January–4 February through 20–24 February) in the top two panels of Figure 1. Fronts are found primarily within interconnected frontal bands generally separated by distances <500 km, and these same bands are outlined by ridges in the $|\nabla T_s|$ field (Fig. 1). We can therefore use these smoothed T_s maps to describe the large-scale distribution and variability of fronts at large horizontal scales during FASINEX.

Although the width and the strength (as measured by $|\nabla T_s|$) of frontal bands partly depend on the degree of smoothing, T_s maps can still be used to study the distribution and variability of frontal bands over the limited range of space scales resolved (e.g., White *et al.*, 1978) as long as the same degree of smoothing is used for each map. T_s variability associated with the variability of these frontal bands can then be studied to help determine the physical processes responsible for frontogenesis, frontolysis, and the advection of existing frontal bands over the limited range of space scales resolved. The processes that lead to frontal formation operate over more than four decades of wavenumber space (and over a wide range of frequencies), and the relative importance of different processes is a function of wavenumber. Results presented in this paper will be valid over less than one full decade of wavenumber space, and will not be
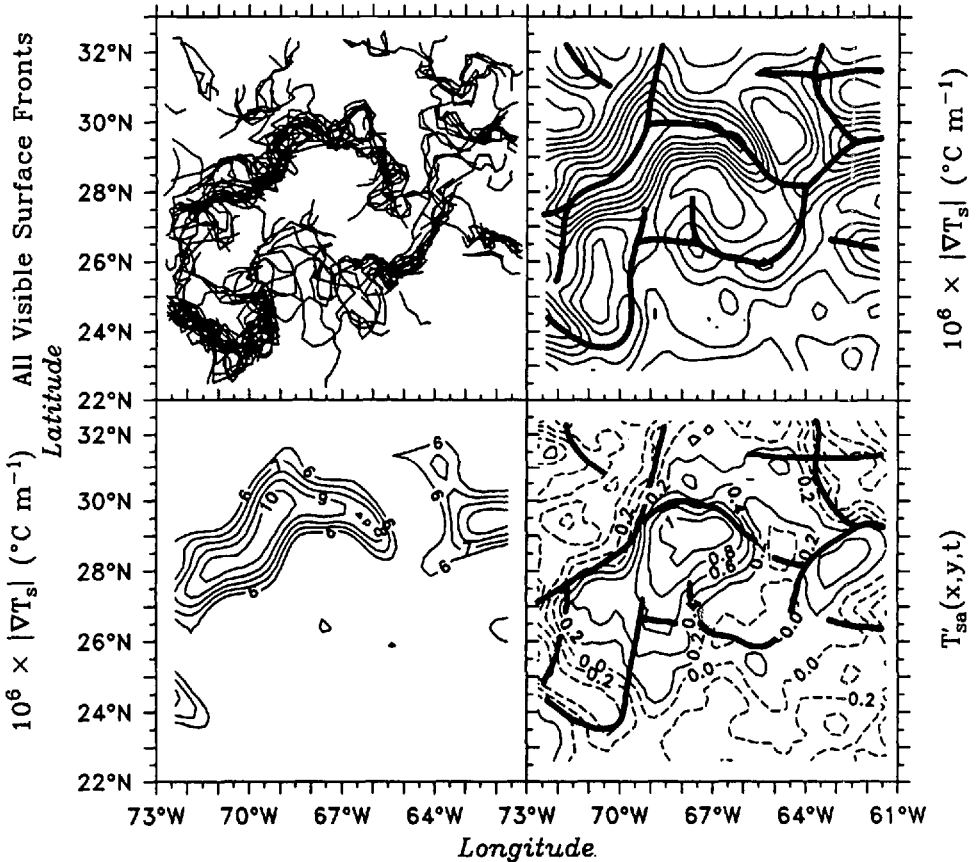
31 Jan. − 4 Feb. to 20−24 Feb.

Figure 1. The locations of all fronts observed in AVHRR images (top left), temperature gradient magnitude ($|\nabla T_s|$) with a contour interval of 1×10^{-6} °C m^{-1} (top right), the same $|\nabla T_s|$ function with a minimum contour threshold set at 6×10^{-6} °C m^{-1} (bottom left), and the anomaly function $T'_{sa}(x, y, t)$ from (4.2) (bottom right), all for the second 25-day interval. Ridges of $|\nabla T_s|$ maxima are traced by dark solid lines in the top right panel, and these lines are reproduced in the bottom right panel.

representative of the processes maintaining the $O(10)$ km frontal interfaces contained within the frontal bands, nor of the processes responsible for the smaller-scale variability of these frontal interfaces.

The existence of a large-scale pattern of interconnected frontal bands within the STCZ has apparently not been well documented, with earlier studies generally concentrating on a single front or frontal band. However, multiple interconnected frontal bands in the upper ocean, with characteristic separation scales of several hundred kilometers, were observed at times by Levine and White (1981) in the North Pacific STCZ using data with coarse resolution (2° latitude × 5° longitude).

In contrast to our observation of characteristic separation distances up to 500 km, Fedorov (1983) identified frontal crossings in several long temperature transects and estimated characteristic frontal separation scales of 40–100 km in major climatic frontal zones of the world ocean, which includes subtropical convergence zones, with the smaller scales prevalent in regions with a relatively energetic eddy field. His estimate is not necessarily inconsistent with ours because fronts will be crossed more frequently than frontal bands, since a ship may encounter more than one front, or a highly-convoluted front more than once, in crossing a frontal band. Also, fronts will be crossed more frequently if a ship sails parallel to a frontal band for a long distance.

b. The SFZ. This picture of multiple interconnected frontal bands is inconsistent with simple conceptual models of the STCZ where wind-driven meridional convergence of heat in the upper-ocean Ekman layer is expected to create a single zonally-oriented subtropical front or frontal zone. A dominant frontal zone can be identified in the 25-day maps, however, by reproducing the contour plot of $|\nabla T_s|$ with a minimum contour threshold set (Fig. 1). Proper selection of this threshold outlines one predominantly zonally-oriented frontal band, which we identify as the SFZ. During the second 25-day interval, the SFZ appears as a band that is oriented zonally to the east of 69W and oriented SW-NE to the west (Fig. 1). It has a break, or relatively weak segment, near 64–65W.

Perturbations in the strength of the SFZ tend to propagate westward (HC1). To illustrate this here, we record the maximum temperature gradient magnitude ($|\nabla T_s|_{max}$) within the SFZ at eleven separate longitudes for all 25-day intervals, then contour it as a function of longitude and time (Fig. 2). The largest values of $|\nabla T_s|_{max}$ are observed between 69 and 72W, and this maximum appears to propagate westward at an average speed of about 1 km day^{-1}. East of 69W, both a minimum and a maximum in $|\nabla T_s|_{max}$ propagate westward at 2–4 km day^{-1}. This propagating signal disappears by May when rapid seasonal warming begins (HC1).

4. Spatial anomaly features

a. Spatial anomaly functions. We calculate 5-day maps of the spatial anomaly function T_{sa} using

$$T_{sa}(x, y, t) = T_s(x, y, t) - T_{sC}(x, y, t), \tag{4.1}$$

where $T_{sC}(x, y, t)$ is the seasonal T_s cycle obtained from the Cooperative Ocean-Atmosphere Data Set (COADS) (Sadler *et al.*, 1987). Monthly fields of T_{sC} were obtained and interpolated to the central times of the 5-day intervals using cubic splines. We average the field of T_{sa} over the 4-month interval from 11–15 January through 11–15 May, prior to the onset of rapid seasonal warming, and contour this temporally-averaged field $[\overline{T}_{sa}(x, y)]$ in Figure 3, correcting for the positive T_s bias documented in HC1. T_s is above normal throughout nearly all of the analysis domain, being about
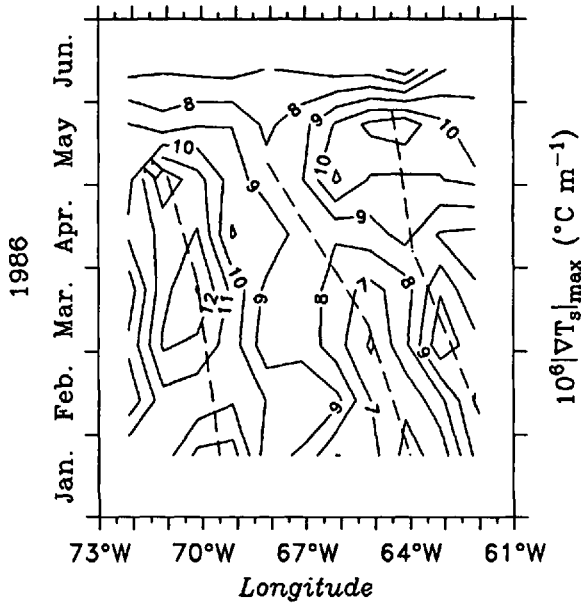
Journal of Marine Research

Figure 2. Contours of $|\nabla T_s|_{max}$ at the latitude of the SFZ contoured as a function of longitude and time. Propagation of extrema is indicated by the dashed lines.

0.8°C above normal near the location of FASINEX mooring F2 and reaching a maximum of about 1.3°C above normal 200–300 km to the northeast (Fig 3). The warm feature centered NE of the FASINEX site is anisotropic, with the major axis oriented SW-NE.

b. Large-scale spatial anomaly features. To isolate T_s variability related to our observed frontal bands, variability with secular space scales must be removed from the T_s maps by least-squares fitting and removing a plane from each map:

$$T'_{sa}(x, y, t) = T_{sa}(x, y, t) - T_0(t) - A(t)x - B(t)y. \qquad (4.2)$$

We contour maps of T'_{sa} in Figure 4 for all eight 25-day intervals. The large anisotropic warm anomaly feature evident in the temporal average of this field between mid-January and mid-May $[\overline{T}'_{sa}(x, y, t)]$ (Fig. 3) is also evident in the first six 25-day maps that span the same time interval (Fig. 4). The major axis of this warm feature is oriented SW-NE, and an anisotropic cold feature with a similar major axis orientation exists to the northwest. Other weaker features are also evident. After mid-May, these features gradually disappear as rapid seasonal warming occurs. They propagate in a predominantly westward direction at a few kilometers per day. For example, the large warm feature is centered near 28.5N, 68W in late January, and near 27.5N 70.5W in early May.

To illustrate the relationship between these anomaly features and the observed
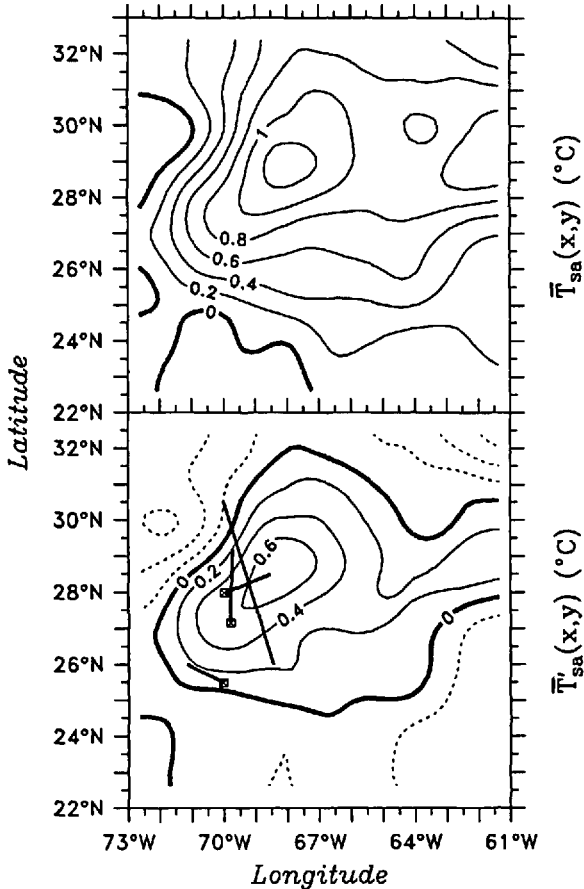
Figure 3. The mean anomaly functions $\overline{T}_{sa}(x, y)$ from (4.1) (top) and $\overline{T'}_{sa}(x, y)$ from (4.2) (bottom) contoured within the analysis domain. The overbar denotes a temporal average between 11–15 January and 11–15 May 1986. A temperature value of 0.58°C was subtracted from the $\overline{T}_{sa}(x, y)$ field to correct for the mean temperature bias described in HC1. Dashed contours indicate negative values. In the bottom panel, four-month vector mean current measured just beneath the base of the mixed layer is plotted for the three FASINEX moorings located at the small squares, which are, from N to S, F1 (162 m), F2 (160 m), and F12 (159 m). The straight line in the bottom panel is the approximate path of the ship-of-opportunity cross-sections used in Fig. 6.

frontal bands, we contour the field of $T'_{sa}(x, y, t)$ for the second 25-day interval in Figure 1, superimposing on it the paths of the ridges of large $|\nabla T_s|$. Some tendency is evident for the frontal bands to exist on the periphery of the warm and cold anomaly features. This pattern is significantly modified, however, by the mean T_s gradient that has been removed from the T'_{sa} field. This causes zonally-oriented frontal bands to be relatively strong between a warm feature to the south and a cold feature to the north, and to be relatively weak or nonexistent between a cold feature to the south and a warm
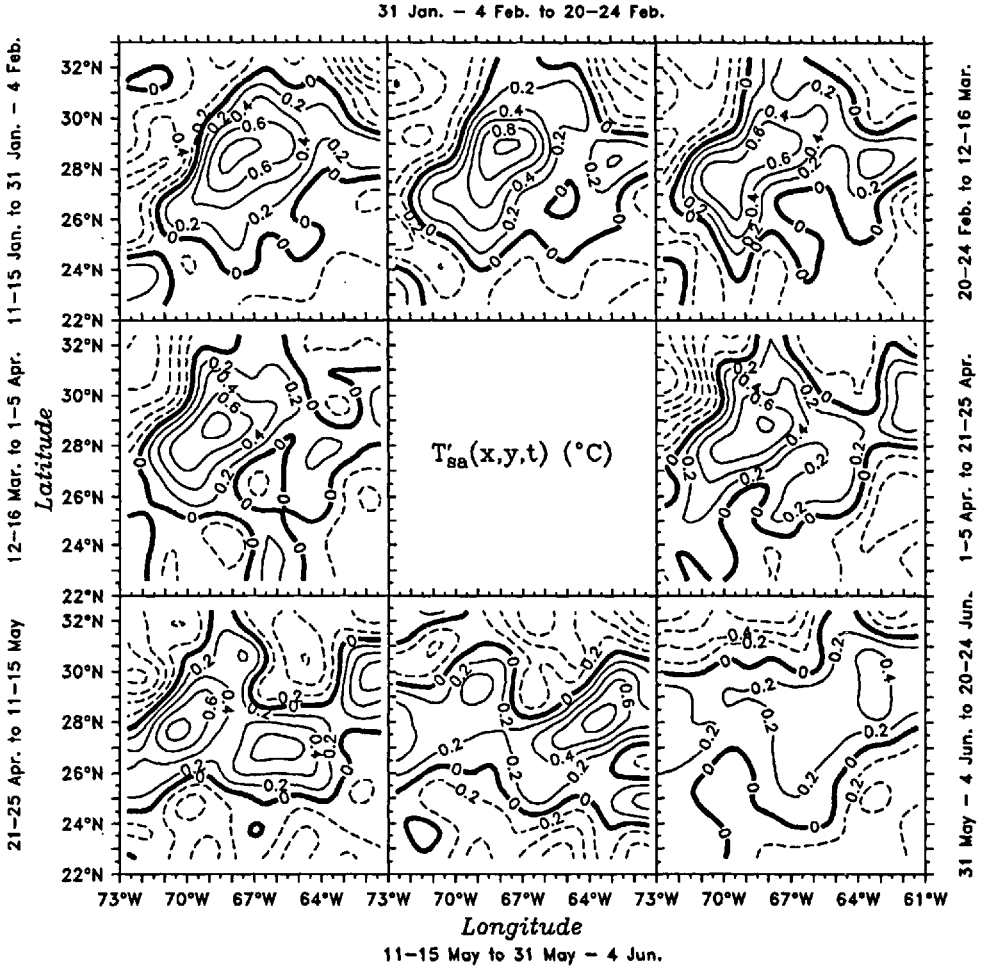
Figure 4. The anomaly function $T'_{sa}(x, y, t)$ from (4.2) contoured for all eight 25-day intervals. Dashed contours indicate negative values.

feature to the north. It is well known that fronts tend to form on the periphery of oceanic eddies, largely due to deformation present in the horizontal current field (Fedorov, 1983), so it is possible that we are observing the influence of underlying eddies on T_s and fronts.

The observed SFZ variability discussed in Section 3b appears to be related to the propagation of the large-scale anomaly features. First, the relatively strong segment of the SFZ to the west of 69W that is evident through mid-May (Fig. 2) separates the large warm anomaly feature in the central part of the analysis domain from the cold anomaly feature to the northwest. The westward propagation of this strong segment (Fig. 2) is apparently related to the westward shift of these two associated anomaly

features (Fig. 4). Also, a cold anomaly feature that is just entering the northeast corner of the analysis domain to the north of 29N in the first 25-day interval can be followed in Figure 4 as it propagates westward, reaching a central longitude of 66–67W by late May. Since a westward-propagating warm anomaly feature exists to the south of this cold feature, the relatively strong segment of the SFZ that exists between them also shifts westward with time (Fig. 2). Fedorov (1983) discusses observations of the westward propagation of fronts associated with mid-ocean eddies that were made during the USSR experiment Polygon-70.

c. Statistical properties of the large-scale anomaly features. To estimate the characteristic time and horizontal space scales of the propagating features, we calculate the three-dimensional autocorrelation function of $T'_{sa}(x, y, t)$ by extending the method of calculating two-dimensional autocorrelation functions described in Halliwell and Allen (1987). The anisotropy of the westward-propagating features is evident in this autocorrelation function (Fig. 5), with the major axis of the central positive correlation ridge rotated about 30° clockwise from the N-S direction at zero lag time. The rate of propagation of the central positive correlation ridge in lag distance space with increasing lag time provides a rough estimate of a characteristic propagation velocity of the features in the field being analyzed, as shown for two-dimensional correlation functions by Halliwell and Mooers (1983) and Halliwell and Allen (1987). The peak within the central positive correlation ridge, initially centered at the origin in lag distance space at zero lag time, shifts westward at 3–4 km day^{-1} up to a lag time of 40 days, after which no single dominant closed peak can be identified. The westward-propagating pattern of ridges and troughs remains evident out to at least 100 days, however. The peak-to-peak space and time scales estimated from this function are ≈800 km (in the minor axis direction) and ≈275 days.

5. Possible forcing mechanisms for the large-scale anomaly features

a. Relationship to internal oceanic variability. We use oceanographic data collected during FASINEX to search for possible relationships between the large-scale T_s anomaly features and internal oceanic variability. Ship-of-opportunity XBT cross-sections were run approximately twice monthly during FASINEX, with temperatures measured to a depth of >800 m at a horizontal spacing averaging about 10 km (Evans *et al.,* 1986). Many of the sections were run along the line connecting 70W, 30.5N to 68.5W, 26N (Fig. 3), and temperatures from three of these sections are contoured in Figure 6. The XBT data were obtained from the National Oceanographic Data Center (NODC), and the data processing is described in Halliwell (1989). To focus on large-scale variability, the XBT data have been meridionally smoothed to remove most of the temperature variance with meridional wavelengths <100–200 km (Halliwell, 1989). Cross-sections of T'_{sa} along the same path are also graphed in Figure 6 for comparison to the XBT sections.
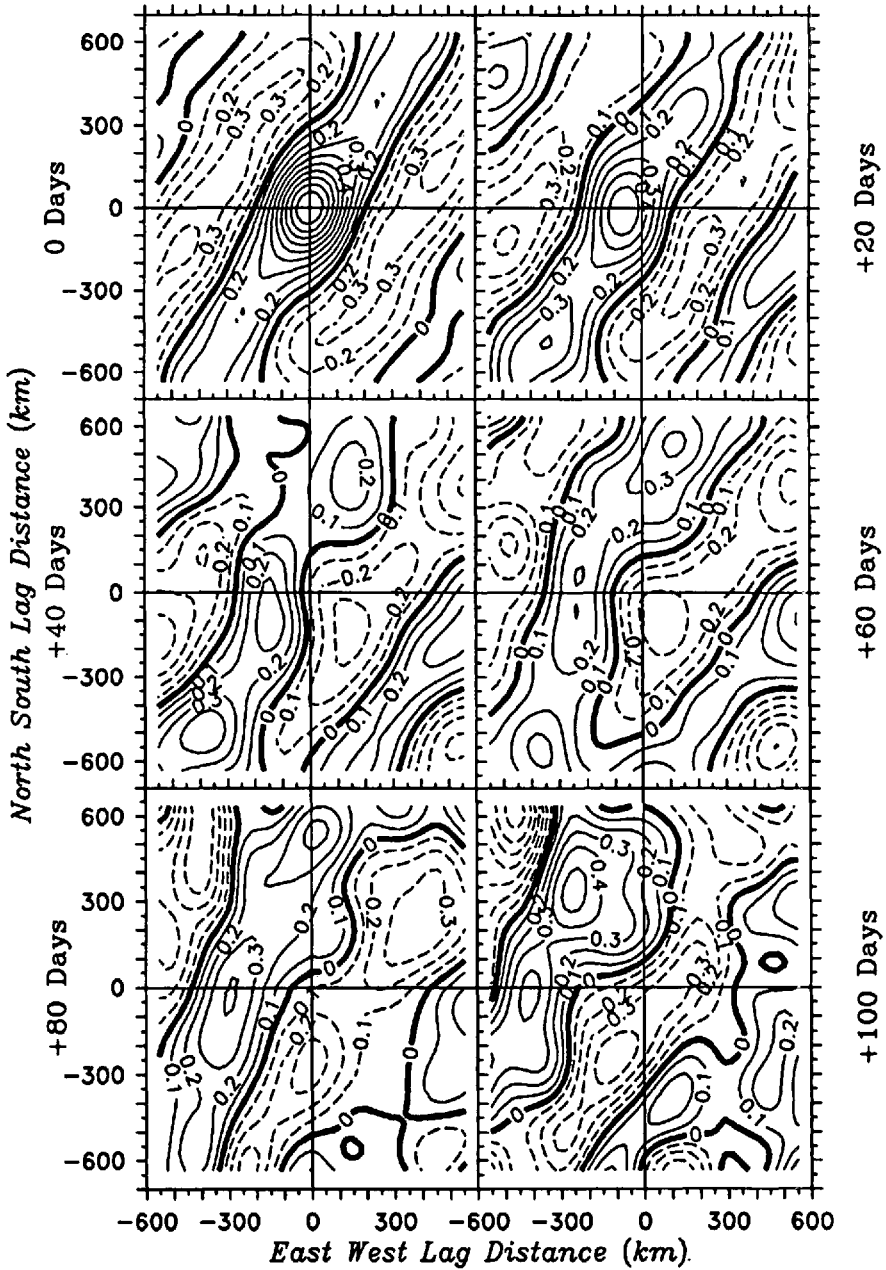
Figure 5. Three-dimensional autocorrelation functions of $T'_{sa}(x, y, t)$ contoured as a function of E-W and N-S lag distances at six different lag times. Dashed contours indicate negative values.
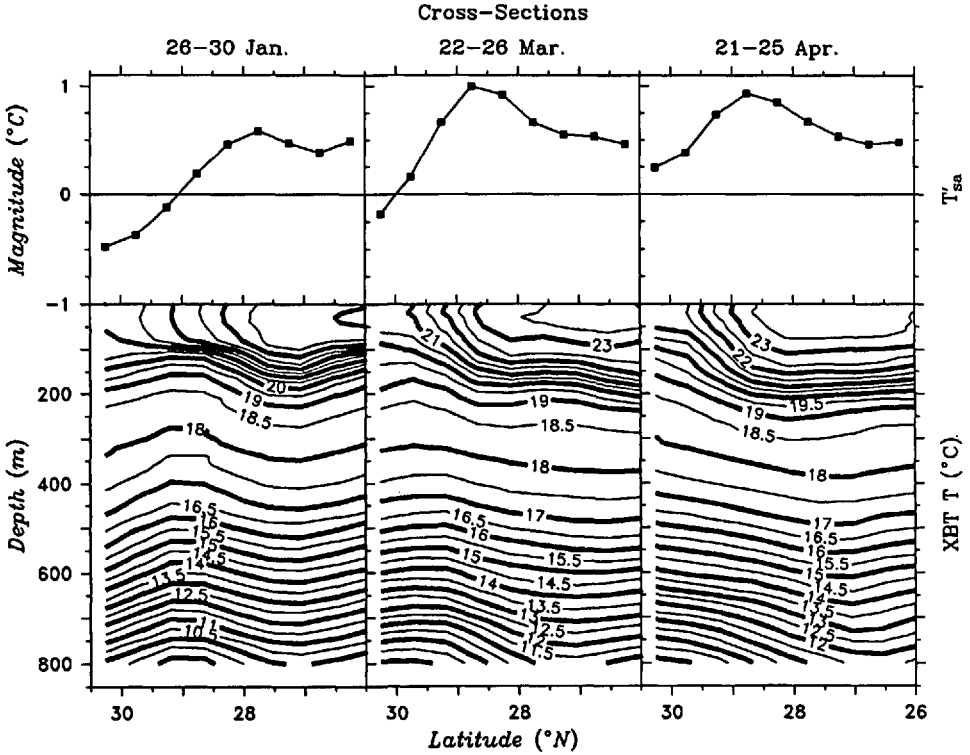
Figure 6. Cross-sections of T'_{sa} (top), and of ship-of-opportunity XBT data (bottom), at three different times. $T'_{sa}(x, y, t)$ was interpolated from the 5-day maps (times shown on top) onto the path of XBT section (Fig. 3) using two-dimensional cubic splines. Each XBT section was run within the corresponding five-day interval. The XBT arrays contoured here have a meridional resolution of 0.5° and a depth resolution of 5 m.

In the first two cross-sections (late January and late March), the southern (northern) part of the path is located within a warm (cold) anomaly feature. Since the major axis of the westward-propagating anomaly features is oriented SW-NE, the anomaly features evident in the T'_{sa} curve shift northward along the XBT path with time until the path is entirely within the warm feature by the time of the third cross-section (late April). The cold and warm anomaly features are visually evident in the XBT mixed layer temperatures. The depths of both the seasonal and main thermoclines tend to vary in phase with T'_{sa} over the horizontal scales of the anomaly features (several hundred kilometers), being shallower (deeper) by up to several tens of meters beneath cold (warm) features, indicating a possible relationship with underlying eddies. The only significant disagreement with this relationship exists at the northern edge of the path in the late-January section where the main thermocline deepens to the north. The deepest parts of the seasonal and main thermoclines are displaced slightly to the south of the latitude of maximum T'_{sa}, so the surface features are not perfectly in-phase

vertically with the deeper temperature variability. The SFZ is easily identified in the XBT cross-sections, and its southern edge coincides with the maximum value of T'_{sa} in all three cross-sections.

If the function T'_{sa} is roughly in-phase vertically with perturbations in the main thermocline, surface geostrophic currents should flow clockwise (anticlockwise) around warm (cold) anomaly features. Vector currents measured just beneath the base of the mixed layer (near 160 m) at moorings F1, F2, and F12 (Pennington *et al.,* 1988; Brink, 1989) have been averaged between mid-January and mid-May and overlayed onto the contour plot of $\overline{T}'_{sa}(x, y, t)$ in Figure 3. The clockwise mean flow around the southwestern part of the strong warm anomaly feature is qualitatively consistent with the above hypothesis. We considered testing if the temporal variability of these currents between mid-January and mid-May reflects the passage of these anomaly features as they propagate westward past the moorings, but our analysis interval is too short to clearly detect any major current reversals caused by the passage of the features, and none are observed in the current records (not shown).

The preceding tests are far too limited to prove that the large-scale T_s anomaly features are roughly vertically in-phase with underlying eddies. However, such a relationship was also supported by analyses of the full two years of FASINEX ship-of-opportunity XBT data (Halliwell, 1989), which demonstrated that temperature variability with meridional scales of a few hundred kilometers was significantly correlated between the surface and the main thermocline (after removing the larger-scale seasonal cycle of upper-ocean temperature) with a meridional phase shift small compared to the scales of the variability. Unfortunately, because of the large space and long time scales of this variability, two years of XBT data spanning 4° of latitude was still insufficient to conclusively prove and accurately characterize this relationship, so it will need to be verified with a data set (including satellite altimetry and subsurface data) that spans a larger region for a longer time interval. For now, we can at least perform some consistency checks in an attempt to discredit this hypothesis. We compare properties of the large-scale anomaly field first to properties of the internal eddy field measured in earlier studies (Section 5b), then to properties of the internal eddy field expected from dynamical considerations (Section 5c).

b. Eddy properties estimated in earlier studies. Eddy properties near or within our analysis domain have been documented in several earlier studies, but they were generally conducted in domains much smaller than ours. For example, the MODE domain is a 250 × 250 km box centered at 69°40'W, 28N (MODE Group, 1978), the POLYMODE Local Dynamics Experiment (LDE) domain is a box about the same size centered near 29N, 70W (Taft *et al.,* 1986), and the 1981 ocean tomography experiment domain is a box about the same size centered near 26N, 70W (Chiu and Desaubies, 1987). In all three of these experiments, the observed eddy field had space scales smaller than those of the T_s anomaly features we observe by about a factor of 2,

but this can be at least partly explained by the difference in domain sizes. Our use of smoothed 25-day T'_{sa} maps to estimate space scales also contributed to the difference. Wherever larger analysis domains have been used, upper-ocean eddies with space scales similar to those of the large-scale T_s anomaly features have generally been observed within subtropical gyres (Leetmaa, 1977; White, 1982; Talley and White, 1987).

Eddies observed in the earlier experiments propagated in a predominantly westward direction at about the speed we observe for the surface anomaly features. The long peak-to-peak temporal scale of $\approx$275 days that we observe coincides with the energetic temporal secular-scale variability (period >150 days) of currents observed during MODE (Schmitz, 1978), although the energy present at these long time scales decreased significantly by the mid-1980's (Schmitz, 1989). These long time scales were also visually evident in 233 m currents measured near 25.5N, 71W between November 1980 and October 1981 (Olson *et al.*, 1984). Spatially anisotropic eddies, with their major axes oriented SW-NE, were observed in MODE and POLYMODE LDE (Shen *et al.*, 1986; Taft *et al.*, 1986). Shen *et al.* (1986) also showed that the T_s field during the LDE was spatially coherent with the dynamic topography of the eddy field between mid-May and mid-June 1978, with relatively warm water found over anticyclones (deeper thermoclines), consistent with what we observe. This relationship disappeared in mid-June after formation of the strong seasonal thermocline. Frankignoul (1981) detected a small, but statistically significant, coherence between T_s and temperature in the main thermocline using a 24-year record of hydrographic stations southeast of Bermuda.

c. Dynamical considerations. If T_s is influenced by eddies with the large space and long time scales of the surface anomaly features we observe, then linear Rossby wave dynamics should describe the properties of this eddy field with reasonable accuracy (e.g. White, 1983). We therefore test whether the properties of the large-scale T_s anomalies are consistent with linear Rossby wave dispersion. Since we did not have subsurface data to resolve the quasigeostrophic wave modes that may be present (e.g. Chiu and Desaubies, 1987), we can only perform a very crude consistency test here. We assume that the lowest baroclinic vertical mode is dominant, and further assume that it consists of a single plane wave with a frequency ω, and a wavenumber vector $\kappa =$ (k, l) normal to (with a westward component) the ridges and troughs of the three-dimensional autocorrelation function (Fig. 5). We assume that ω and $|\kappa|$ equal the inverse of the peak-to-peak scale estimates made from the three-dimensional autocorrelation functions (Section 4c). We estimate phase velocity magnitude $|c_p|$ from the rate that the central positive correlation ridge shifts in lag distance space with increasing lag time. All of these parameter estimates, which are listed in Table 1, are rough because Rossby waves are dispersive and we have sampled the large-scale T_s anomaly features only over about 1/2-2 cycles in time and 1-3 cycles in space. The

Table 1. Rossby wave dispersion parameters estimated from the T_s anomaly field using the three-dimensional autocorrelation functions in Figure 5. All direction angles are in degrees anticlockwise from due east.

Parameter	Estimate
$\|\kappa\|$ (m^{-1})	7.85×10^{-6}
k (m^{-1})	-6.80×10^{-6}
l (m^{-1})	3.93×10^{-6}
a (m)	4.40×10^4
ω (s^{-1})	2.64×10^{-7}
ω_{max} (s^{-1})	4.44×10^{-7}
$\|c_p\|$ (km day^{-1})	2.90
$\theta_p = \theta_{\|\kappa\|}$ (deg)	150
$c_p^{(x)}$ (km day^{-1})	-2.51
$c_p^{(y)}$ (km day^{-1})	1.45
$\|c_g\|$ (km day^{-1})	3.42
θ_g (deg)	186
$c_g^{(x)}$ (km day^{-1})	-3.40
$c_g^{(y)}$ (km day^{-1})	0.35

frequencies that we estimate could be Doppler-shifted by a larger-scale mean current which cannot be estimated with available data (Killworth, 1979). Even if the surface anomaly features are coupled to underlying eddies, the surface features will probably not be perfect tracers of these eddies. Out of necessity, we assume that the estimated parameters represent those of a dominant wave in the system and that these estimates are adequate for the crude consistency tests presented here.

We can now make two consistency tests. Using estimates of k and ω, we calculate the value of the Rossby radius a from the dispersion relation to determine if it has a realistic magnitude. We also estimate the maximum permissible frequency of Rossby waves at a latitude of 27.5N to determine if the frequencies we observe are smaller than this limit. Since $|\kappa|$ was found to be $\ll a^{-1}$, we use the long wave approximation to the Rossby wave dispersion relation (Gill, 1982):

$$\omega = -\beta k a^2. \tag{5.1}$$

The maximum permissible frequency is given by

$$\omega_{max} = \frac{\beta a}{2}. \tag{5.2}$$

We can also estimate the group velocity using

$$\mathbf{c}_g = (c_g^{(x)}, c_g^{(y)}) = -\beta(a^2, 2kla^4) \tag{5.3}$$

allowing us to speculate on where these waves, assuming they actually exist and do affect T_s, are generated.

The estimate of the Rossby radius is 44 km, close to the estimate of 45 km by Brink

(pers. commun.), while the maximum permissible frequency is about 70% larger than the estimated frequency (Table 1). The magnitudes of the phase and group velocities are 2.90 and 3.42 km day^{-1}, while the directions of the phase and group velocities [θ_{c_p} and θ_{c_g}] are 150° and 186° (anticlockwise from due east). Chiu and Desaubies (1987) obtained similar group velocities from their first-mode baroclinic wave fits using ocean tomography experiment data. If T_s is being influenced by underlying large-scale eddies, their source must be to the east of the analysis domain and not near the Gulf Stream.

d. Possible atmospheric forcing mechanisms. We searched for evidence of local coupling between wind stress fluctuations and the large-scale T_s anomalies by calculating three-dimensional cross-correlation functions between atmospheric forcing fields (FNOC wind stress components and wind stress curl) and the $T'_{sa}(x, y, t)$ field. The basic statistical properties of the atmospheric forcing fields used are described in HC1. The cross-correlation magnitudes between the three wind stress variables and T'_{sa} (not shown) are all small and insignificant. An attempt was made in HC2 to detect the expected response of the SFZ and its associated T_s perturbations to wind-driven horizontal heat advection in the Ekman layer. They showed that the westward propagation of the large-scale T_s spatial anomaly features had the dominant influence on T_s and the SFZ at these scales during FASINEX. The response to Ekman advection could only be marginally detected by zonally-averaging terms of the upper-ocean heat balance across the entire analysis domain, which effectively averaged out most of the influence of the propagating anomaly features.

Even if underlying eddies are responsible for most of the large-scale T_s variability, atmospheric forcing could still be indirectly important. Rossby wave fields with space scales, time scales, and propagation velocities similar to those of the spatial anomaly features we observe can theoretically be generated by wind stress curl fluctuations with these long time scales interacting with an eastern boundary of an ocean basis (e.g. Cummins *et al.*, 1986; Reason *et al.*, 1987), or interacting with the mid-Atlantic ridge (Barnier, 1988). Numerical model solutions in the latter study consist of a westward-propagating wave field generated at the ridge by the annual cycle of wind stress curl. This wave field is anisotropic and has a major axis orientation similar to that which we observe. Frankignoul and Müller (1979) and Müller and Frankignoul (1981) show that an internal eddy field can be generated over the open ocean in the absence of topography that can account for some of the observed eddy variability in the western North Atlantic STCZ. Unfortunately, we cannot determine how important these forcing mechanisms are using available data. All of these models predict poor local coherence between atmospheric forcing and the eddy response.

6. Discussion

During FASINEX, fronts in the western North Atlantic STCZ tended to be found within distinct interconnected bands separated by up to 500 km. These bands tended to

be located on the periphery of westward-propagating large-scale T_s anomaly features. Much of the variability of the dominant zonally-oriented frontal zone (the SFZ) was related to the propagation of these features, which made it difficult to detect the expected response of the SFZ to the meridional convergence of Ekman transport (HC2). We could not statistically detect any local coupling between these features and wind stress or wind stress curl. They propagated at about 3 km day^{-1} in a predominantly westward direction, had peak-to-peak time scales of ≈ 275 days, and were strongly anisotropic with a major axis oriented SW-NE. Peak-to-peak horizontal scales in the minor axis direction were about 800 km, while scales in the major axis direction were much larger than the size of the analysis domain. These features persisted with relatively small changes in structure and amplitude from mid-January through mid-May 1986, but they disappeared shortly thereafter due to the strong surface heat flux and seasonal thermocline formation. A warm anomaly feature moved slowly past the FASINEX moorings during the experiment, and T_s was consequently $\approx 1°C$ above normal at the location of the FASINEX moorings during the experiment.

Limited oceanographic data from XBT cross-sections indicated that both the seasonal and main thermoclines tended to be shallower (deeper) beneath cold (warm) anomaly features, but we had insufficient data coverage to prove whether this relationship was statistically significant in our analyses presented here. This relationship was more strongly (but still not conclusively) supported by analyses of two years of FASINEX ship-of-opportunity XBT cross-sections presented in Halliwell (1989). It is therefore possible that T_s is being influenced in some manner by underlying baroclinic eddies at the large scales of the observed surface anomaly features. We compared observed properties of the anomaly features to theoretically-expected properties of large-scale eddies, and also to properties of the eddy field measured in earlier studies, and could find no evidence to discredit this hypothesis.

If this hypothesis is true, what are the physical mechanisms that couple mixed-layer temperature to the eddy field beneath? The formation of T_s anomalies due to mesoscale eddies was observed during MODE (Voorhis *et al.*, 1976), where the horizontal currents advected tongues of warm water northward and cold water southward around the edges of the eddies. These tongues were substantially smaller than the anomaly features we observed. They also were substantially out-of-phase vertically with the associated thermocline perturbations, not close to being in-phase as we observed. This suggests that other mechanisms must be significant at the large scales we resolve. For example, Stevenson (1983) describes how an internal Rossby wave field can affect the vertical advection of heat at the base of the mixed-layer, while Klein and Hua (1988) show that an existing internal quasigeostrophic eddy field can modulate the mixed-layer response to atmospheric forcing to produce T_s anomalies that are related to the underlying eddy field. We could not quantitatively evaluate the importance of these mechanisms with available data.

In summary, we have successfully documented many properties of the large-scale

distribution and variability of frontal bands, and also of the large-scale T_s anomaly features associated with these bands, during FASINEX. Unfortunately, these anomaly features were dominated by such large space and time scales, we could not resolve their properties very accurately. Therefore, the possible relationship between T_s and internal oceanic eddies that we document here must be tested in future experiments. We are presently extending our meteorological and T_s data set in both space and time (1982–88), and obtaining other measurements of oceanic variability, including satellite altimetry and subsurface measurements, for future analyses to test this hypothesis. This will also enable us to determine how typical the observed variability during FASINEX was.

REFERENCES

Barnier, B. 1988. A numerical study on the influence of the Mid-Atlantic Ridge on non-linear first-mode baroclinic Rossby waves generated by seasonal winds. J. Phys. Oceanogr., *18*, 417–433.

Böhm, E. 1988. Subtropical fronts in the Sargasso Sea: a four-year satellite analysis. M.S. thesis, Graduate School of Oceanography, University of Rhode Island, Narragansett, RI, 61 pp.

Brink, K. H. 1989. Evidence for wind-driven current fluctuations in the western North Atlantic. J. Geophys. Res., *94*, 2029–2044.

Chiu, C-S. and Y. Desaubies. 1987. A planetary wave analysis using the acoustic and conventional arrays in the 1981 ocean tomography experiment. J. Phys. Oceanogr., *17*, 1270–1287.

Cummins, P. F., L. A. Mysak and K. Hamilton. 1986. Generation of annual Rossby waves in the North Pacific by the wind stress curl. J. Phys. Oceanogr. *16*, 1179–1189.

Evans, D. L., G. A. Strout and A. K. Monaghan. 1986. FASINEX ship-of-opportunity data report. Tech. Rep. Ref. No. 86-6, Graduate School of Oceanography, University of Rhode Island, Narragansett, Rhode Island.

Fedorov, N. K. 1983. The physical nature and structure of oceanic fronts. Lect. Notes on Coast. and Estuar. Stud., *19*, N. Demidenko, Translator, C. Garrett, Tech. Ed., Springer-Verlag, Berlin, 333 pp.

Frankignoul, C. 1981. Low-frequency temperature fluctuations off Bermuda. J. Geophys. Res., *86*, 6522–6528.

Frankignoul, C. and P. Müller. 1979. Quasi-geostrophic response of an infinite β-plane ocean to stochastic forcing by the atmosphere. J. Phys. Oceanogr., *9*, 104–127.

Gill, A. E. 1982. Atmosphere-Ocean Dynamics. Academic Press, New York, 662 pp.

Halliwell, Jr., G. R. 1989. Ship-of-opportunity cross-sections of the western North Atlantic subtropical convergence zone. J. Geophys. Res., (in press).

Halliwell, Jr., G. R. and J. S. Allen. 1987. Wave number-frequency domain properties of coastal sea level response to alongshore wind stress along the west coast of North America 1980–84. J. Geophys. Res., *92*, 11761–11788.

Halliwell, Jr., G. R. and P. Cornillon. 1990a. Large-scale SST variability in the western North Atlantic subtropical convergence zone during FASINEX, part 1: Description of SST and wind stress fields. J. Phys. Oceanogr., (in press).

—— 1990b. Large-scale SST variability in the western North Atlantic subtropical convergence zone during FASINEX, part 2: Upper ocean heat balance and frontogenesis. J. Phys. Oceanogr., (in press).

Halliwell, Jr., G. R. and C. N. K. Mooers. 1983. Meanders of the Gulf Stream downstream from Cape Hatteras, 1975–1978. J. Phys. Oceanogr., *13*, 1275–1292.

Killworth, P. 1979. On the propagation of stable baroclinic Rossby waves through mean shear flow. Deep-Sea Res., *26A*, 997–1031.

Klein, P. and B. L. Hua. 1988. Mesoscale heterogeneity of the wind-driven mixed layer: influence of a quasigeostrophic flow. J. Mar. Res., *46*, 495–525.

Leetmaa, A. 1977. Observations of large-scale depth perturbations of the main thermocline. J. Phys. Oceanogr., *7*, 746–748.

Leetmaa, A. and A. D. Voorhis. 1978. Scales of motion in the subtropical convergence zone. J. Geophys. Res., *83*, 4589–4592.

Levine, E. R. and W. B. White. 1981. Large-scale synoptic thermal fronts in the mid-latitude North Pacific. J. Geophys. Res., *86*, 6567–6579.

MODE Group. 1978. The Mid-Ocean Dynamics Experiment. Deep-Sea Res., *25*, 859–910.

Müller, P. and C. Frankignoul. 1981. Direct atmospheric forcing of geostrophic eddies. J. Phys. Oceanogr., *11*, 287–308.

Niiler, P. P. and R. W. Reynolds. 1984. The three-dimensional circulation near the eastern North Pacific subtropical front. J. Phys. Oceanogr., *14*, 217–230.

Olson, D. B., F. A. Schott, R. J. Zantopp and K. D. Leaman. The mean circulation east of the Bahamas as determined by a recent measurement program and historical XBT data. J. Phys. Oceanogr., *14*, 1470–1487.

Pennington, N. J., R. A. Weller and K. H. Brink. 1988. FASINEX moored current meter array data report. WHOI Tech. Rep. 88-63, Woods Hole Oceanographic Institution, Woods Hole, MA.

Reason, C. J. C., L. A. Mysak and P. F. Cummins. 1987. Generation of annual period Rossby waves in the South Atlantic Ocean by the wind stress curl. J. Phys. Oceanogr., *17*, 2030–2042.

Roden, G. I. 1980. On the subtropical front north of Hawaii during winter. J. Phys. Oceanogr., *10*, 342–362.

Sadler, J. C., M. A. Lander, A. M. Hori and L. K. Oda. 1987. Tropical marine climate atlas, Volume 1: Indian Ocean and Atlantic Ocean. Tech. Rep. UHMET 87-01, Department of Meteorology, University of Hawaii, Honolulu, Hawaii.

Schmitz, W. J., Jr. 1978. Observations of the vertical distribution of low-frequency kinetic energy in the western North Atlantic. J. Mar. Res., *36*, 295–310.

—— 1989. The MODE site revisited. J. Mar. Res., *47*, 131–151.

Shen, C. Y., J. C. McWilliams, B. A. Taft, C. C. Ebbesmeyer and E. J. Lindstrom. 1986. The mesoscale spatial structure and evolution of dynamical and scalar properties observed in the northwestern Atlantic Ocean during the POLY-MODE Local Dynamics Experiment. J. Phys. Oceanogr., *16*, 454–482.

Stage, S. A. and R. A. Weller. 1985. The Frontal Air-Sea Interaction Experiment (FASINEX); Part I: Background and scientific objectives. Bull. Amer. Meteor. Soc., *66*, 1511–1520.

—— 1986. The Frontal Air-Sea Interaction Experiment (FASINEX); Part II: Experimental plan. Bull. Amer. Meteor. Soc., *67*, 16–20.

Stevenson, J. W. 1983. The seasonal variation of the surface mixed layer response to the vertical motion of linear Rossby waves. J. Phys. Oceanogr., *13*, 1255–1268.

Taft, B. A., E. J. Lindstrom, C. C. Ebbesmeyer, C. Y. Shen and J. C. McWilliams. 1986. Water mass structure during the POLYMODE Local Dynamics Experiment. J. Phys. Oceanogr., *16*, 403–426.

Talley, L. D. and W. B. White. 1987. Estimates of time and space scales at 300 meters in the midlatitude North Pacific from the TRANSPAC XBT program. J. Phys. Oceanogr., *17*, 2168–2188.

Van Woert, M. L. 1982. The subtropical front: satellite observations during FRONTS 80. J. Geophys. Res., *87*, 9523–9536.

—— 1983. Satellite observations of fronts and frontal meanders in the central North Pacific Ocean. PhD dissertation, Scripps Institution of Oceanography, La Jolla, CA, 113 pp.

Voorhis, A. D. 1969. The horizontal extent and persistence of thermal fronts in the Sargasso Sea. Deep-Sea Res., *16* (Suppl.), 331–337.

Voorhis, A. D., E. H. Schroeder and A. Leetmaa. 1976. The influence of deep mesoscale eddies on the sea surface temperature in the North Atlantic subtropical convergence. J. Phys. Oceanogr., *6*, 953–961.

Voorhis, A. D. and J. G. Bruce. 1982. Small-scale surface stirring and frontogenesis in the subtropical convergence of the western North Atlantic. J. Mar. Res., *40* (Suppl.), 801–821.

White, W. B. 1982. Travelling wave-like mesoscale perturbations in the North Pacific current. J. Phys. Oceanogr., *12*, 231–243.

—— 1983. Westward propagation of short-term climatic anomalies in the western North Pacific Ocean from 1964–1974. J. Mar. Res., *41*, 113–125.

White, W. B., K. Hasunuma and H. Solomon. 1978. Large-scale seasonal and secular-scale variability of the subtropical front in the western North Pacific from 1954–1974. J. Geophys. Res., *83*, 4531–4544.